MTLA 30 (2023) 101801

Contents lists available at ScienceDirect

Materialia

journal homepage: www.elsevier.com/locate/mtla

Boron trapping at dislocations in an additively manufactured polycrystalline superalloy

Stoichko Antonov [a,1], Arthur Després [b], Charlotte Mayer [c], Guilhem Martin [b], Paraskevas Kontis [d,*]

[a] Max-Planck-Institut für Eisenforschung GmbH, Max-Planck-Strasse 1, 40237 Düsseldorf, Germany
[b] Univ. Grenoble Alpes, CNRS, Grenoble INP, SIMaP, F-38000 Grenoble, France
[c] Aubert et Duval, Usine des Ancizes, Rue des villas, BP1, 63770 Les Ancizes, France
[d] Department of Materials Science and Engineering, NTNU Norwegian University of Science and Technology, 7034 Trondheim, Norway

ARTICLE INFO

Keywords:
Additive manufacturing
Nickel-based superalloys
Dislocations
Boron

ABSTRACT

Segregation of solutes at dislocations in a nickel-based superalloy produced by laser powder bed fusion was investigated. Transmission electron microscopy has shown a high dislocation density present in the as-built microstructure, which was significantly reduced after a subsolvus heat-treatment, but not completely removed. Atom probe tomography revealed segregation of boron at dislocations in the γ matrix in the as-built state. Such segregation was observed for dislocations both in the interdendritic and dendritic core region, but also for dislocations close to grain boundaries. Molybdenum, carbon and tungsten were also found to segregate at dislocations in the γ matrix. After the subsolvus heat treatment, the segregation behaviour of dislocations remaining in the γ matrix is not altered. Boron, molybdenum and tungsten were found to segregate at dislocations but at higher amounts compared to those in the as-built state. Ramifications of boron trapping at dislocations in additively manufactured superalloys are briefly discussed.

1. Introduction

Boron in additively manufactured superalloys is a double-edged sword. It is well known that boron is the main grain boundary strengthening solute in polycrystalline superalloys [1–3]. In its absence, polycrystalline superalloys fail to achieve the required creep and fatigue performance at elevated temperatures [4,5]. Depending on the amount of boron and the grain size of the alloy, boron is often observed to segregate at grain boundaries or partition in borides, leading to various mechanisms responsible for the so-called boron effect in superalloys [6–11]. However, it is known that weldability difficulties can arise in the presence of boron [12], where hot cracking prevails for instance during the repair process of the superalloy. The challenge of avoiding hot cracks due to the presence of boron also exists in superalloys attempted to be produced by additive manufacturing routes [13–18]. If this challenge is not addressed, there might be a limited use of additive manufacturing (AM) processes to produce polycrystalline superalloys. Thus, there is a need to further explore and understand the partitioning behaviour of boron in such processes, aiming to enable crack-free additively manufactured superalloys, without compromising their grain boundary strength at elevated temperatures.

To better understand the partitioning of boron, it is also important to consider the interaction and segregation of boron at crystal defects, such as dislocations and stacking faults. Recently, it was shown that such interactions alter the composition of superalloys during deformation at elevated temperatures, and thus control their microstructural evolution [19]. Often in superalloys produced by Laser Powder Bed Fusion (L-PBF), the as-built microstructure contains a high dislocation density in a super-saturated matrix, where segregation of solutes at interdendritic and dendritic regions is reported [15,17,20,21]. However, no studies have been performed to investigate potential segregation of solutes, including boron, at dislocations in AM produced superalloys.

Here, we provide new insights into the partitioning character of boron by revealing segregation of boron at dislocations in a nickel-based superalloy produced by laser powder bed fusion (L-PBF). Transmission electron microscopy and atom probe tomography have been used to study as-built and heat-treated specimens, in which the segregation of boron amongst other solutes is observed. Possible consequences of boron

* Corresponding author.
E-mail address: paraskevas.kontis@ntnu.no (P. Kontis).
[1] Now at: National Energy Technology Laboratory, 1450 Queen Avenue SW, Albany, OR 97321, USA.

https://doi.org/10.1016/j.mtla.2023.101801
Received 23 December 2022; Accepted 22 May 2023
Available online 23 May 2023
2589-1529/© 2023 The Author(s). Published by Elsevier B.V. on behalf of Acta Materialia Inc. This is an open access article under the CC BY license (http://creativecommons.org/licenses/by/4.0/).

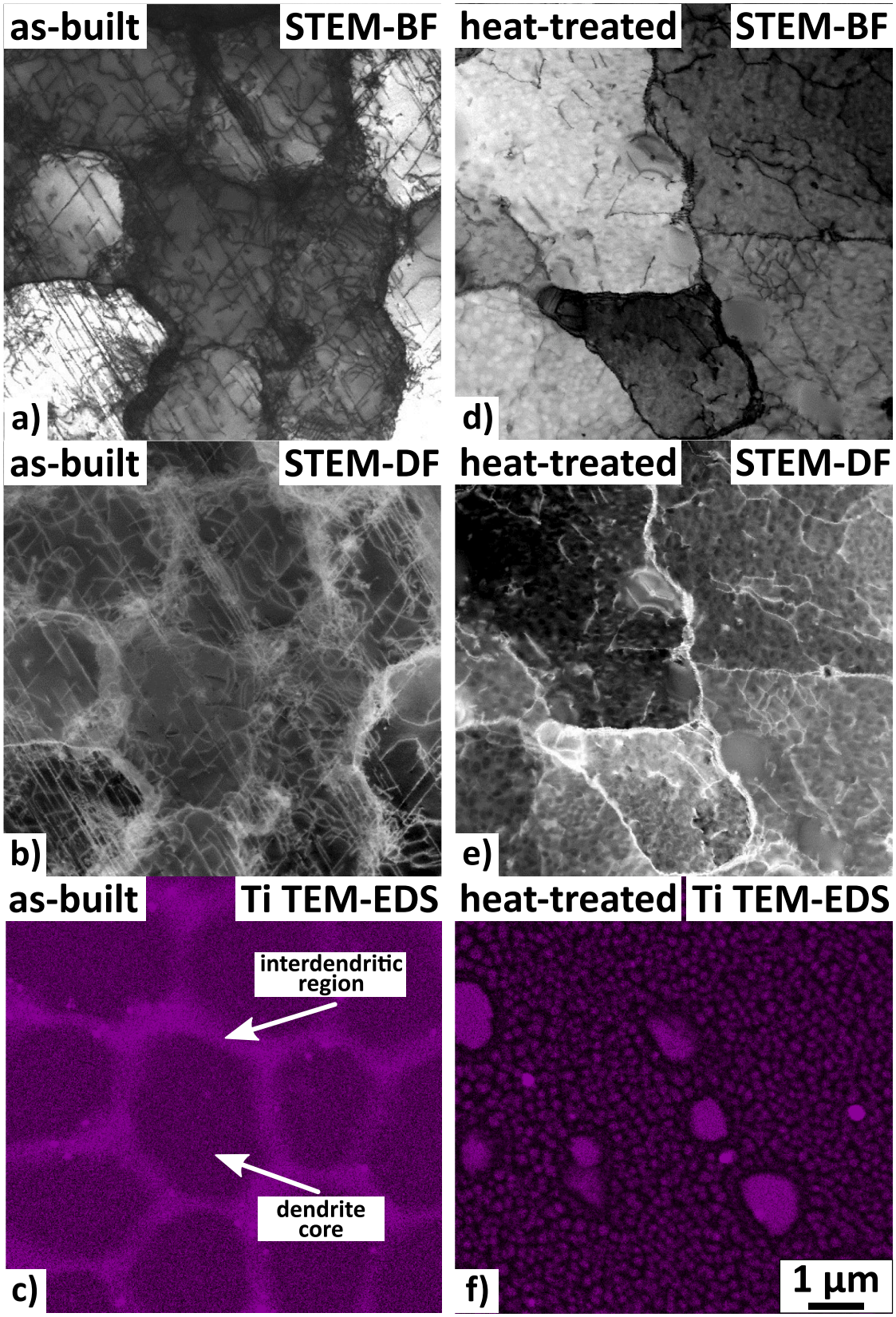

Fig. 1. Bright and dark field STEM micrographs alongside corresponding TEM-EDX maps of titanium from the as-built (a-c) and fully heat-treated (d-f) microstructure of AD730.

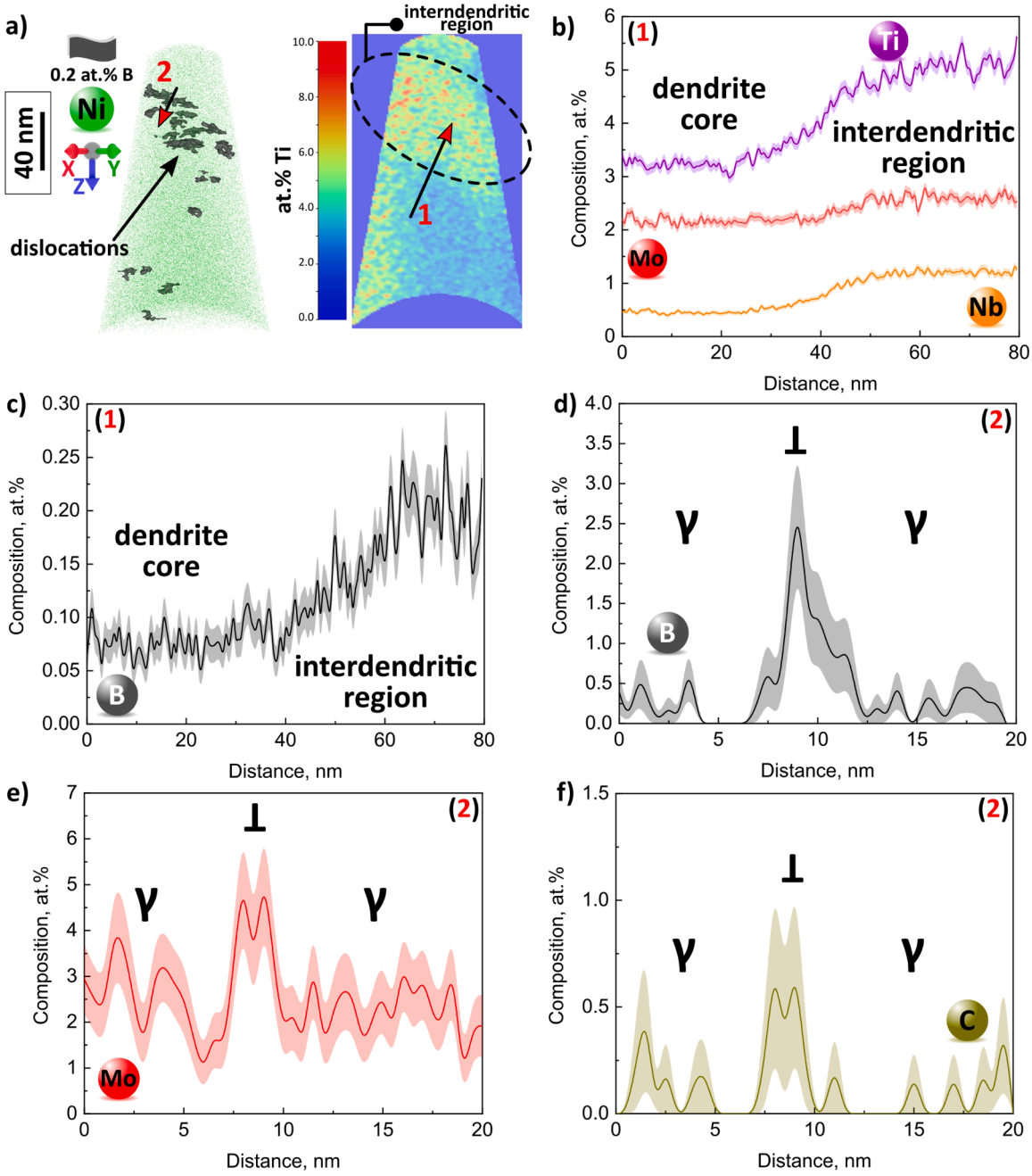

Fig. 2. a) APT reconstruction from the as-built sample from the cellular microstructure showing dislocations, alongside a 2D contour map of Ti revealing the interdendritic region. b), c) 1D composition profiles across the interdendritic region shown in Fig. 2a and denoted by arrow #1. 1D composition profiles across the dislocation denoted by arrow #2 in Fig. 2a of d) boron, e) molybdenum and f) carbon. Error bars are shown as lines filled with colour and correspond to the 2σ counting error.

segregation at dislocations are briefly discussed.

2. Experimental procedures

2.1. Material

The polycrystalline nickel-based superalloy AD730® with composition Ni-17.6Cr-8.3Co-4.2Fe-1.8Mo-0.8W-5.1Al-3.7Ti-0.7Nb-0.1C-0.05B-0.03Zr (at.%) provided in powder form by Aubert et Duval was investigated. An EOS M290 machine was used to produce rectangular samples with dimensions of 70 × 13 × 10 mm (length-width-height) by L-PBF. The linear energy density, defined as laser power divided by scan speed, was set to 0.38 J/mm. The hatch spacing was 100 μm, and the laser scan direction was rotated by 67° between each deposited layer. All the builds were performed under an argon atmosphere. Following the L-PBF deposition, the samples were first solution heat-treated at 1080 °C for 4 h (sub-solvus solution) and subsequently aged at 760 °C for 16 h. The heat-treatment stages were performed in air.

2.2. Transmission electron microscopy

In order to investigate the dislocation density, the as-built and fully heat-treated samples were characterized by transmission electron microscopy (TEM). Thin foils were observed in a FEG JEOL 2100F operating at 200 kV. Bright-field (BF) and dark-field (DF) images were acquired in the scanning transmission electron microscopy (STEM)

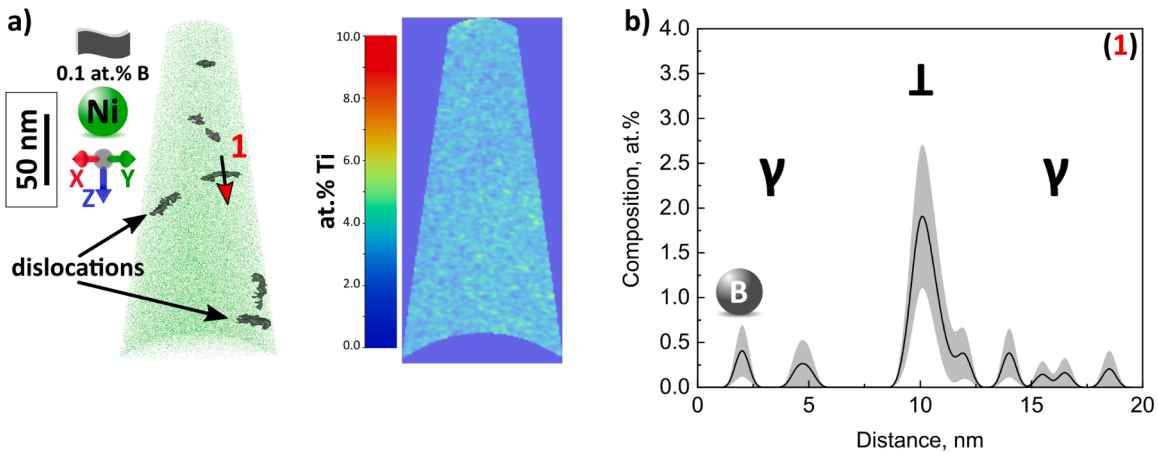

Fig. 3. a) APT reconstruction from the as-built sample from a dendritic core showing dislocations, alongside a 2D contour map of Ti. b) 1D composition profile of boron across the dislocation denoted by arrow #1 in Fig. 3a. Error bars are shown as lines filled with colour and correspond to the 2σ counting error.

mode. All observations were carried out in $[110]_\gamma$ zone axes. As titanium is expected to segregate at interdendritic spacings, and be depleted in the dendrite cores [22], it was used to distinguish the dendrite cores from the interdendritic spacings. Titanium segregation was mapped by energy dispersive X-ray spectroscopy (EDX), using a Silicon Drift Detector Centurio detector. The Kα emission energy was used for detection.

2.3. Atom probe tomography

In search for proof of solutes segregating at dislocations during the L-PBF, atom probe tomography (APT) was used. In particular, APT was performed in specific regions in the as-built sample. Specimens were extracted from both the interdendritic and the dendrite core regions. Similarly, APT samples were prepared from within the grains in the heat-treated sample aiming to study potential segregation of solutes at dislocations remaining after the heat treatment. A FEI dual beam focused ion beam (FIB) Helios 600i was used to prepare the APT samples from site-specific lift-outs, following procedures described in Ref [23]. A Cameca LEAP 5000 XR instrument was used to analyse the APT samples, operated in laser mode at 60 K, with a repetition rate at 125 kHz and with laser energy at 45pJ. Data reconstruction and processing was performed using the AP Suite 6.1 software tool.

3. Results and discussion

3.1. Dislocations in as-built and heat treated microstructure

Figure 1 shows BF- and DF-STEM images from the as-built and fully heat-treated microstructures of the L-PBF produced alloy. In particular, in the case of the as-built microstructure cellular dendrites are clearly observed, alongside elemental segregation of titanium at the interdendritic regions, as shown in Fig. 1. These interdendritic regions are often found to be decorated by dislocation arrays in microstructures inherited from L-PBF [20,24]. Although, dislocations are observed at both dendrite core and interdendritic regions, a much higher dislocation density is observed in the interdendritic regions, while straight dislocations are observed in the dendrite core. Note, that γ′ precipitates are not observed within the cellular dendrites after L-PBF. After the full heat-treatment, the dislocation density is significantly reduced, as shown in Fig. 1d and 1e. Although, the dislocation density is reduced, several dislocations are still visible within the microstructure. Apart from the dislocations, γ′ precipitates with two distinct sizes are now clearly visible following the heat treatment ageing, which can be seen in Fig. 1f. After the full heat treatment, the microsegregation of titanium inherited from solidification observed in the as-built case has been removed. We only see the well-known partitioning between the γ and γ′ phases.

3.2. Trapping of boron at dislocations

Potential segregation of solutes at dislocations was investigated by APT. Similar studies on superalloys produced by traditional processing routes have revealed segregation of solutes at crystal defects, such as dislocations and stacking faults, generated after plastic deformation at elevated temperatures [19]. Fig. 2 shows an APT reconstruction from the as-built microstructure. In particular, in Fig. 2a, both the dendrite core and the interdendritic regions are observed, as revealed by the 2D contour map of Ti. In particular, a region within the analysed APT volume with a higher amount of titanium (Ti ≈ 5 at.%) is found, which is in agreement with the Ti microsegregation observed by EDS in Fig. 1c, but also with previous reports [25,26]. Fig. 2b shows a 1D composition profile across that region, as indicated by arrow #1 in Fig. 2a, and it clearly shows the segregation of Ti, indicating the interdendritic region within the analysed volume. Nb partitioning in the interdendritic regions is also observed but is less pronounced than for Ti. A very slight Mo enrichment in the interdendritic spaces can also be detected. Those observations are in qualitative agreement with the partitioning behaviour of such solutes during solidification of superalloys [27,28]. Note that given the high solid-liquid interface velocity taking place during L-PBF, there could be slight differences in the solute segregation profile of some elements compared to the expectation from simulations based on the Scheil-Gulliver model. Besides, Fig. 2c shows an enrichment of boron at the interdendritic region compared to the dendritic core. This observation of B partitioning in the interdendritic regions is in agreement with previous experimental studies and solidification thermodynamic calculations, see e.g. [17,26,29]. Indeed, B is rejected in the residual liquid films during the last stages of solidification, thus the interdendritic regions are enriched in B.

In the interdendritic region tubular features that correspond to segregation at dislocations are observed, in agreement with the high density of dislocations as shown in Fig. 1. Such features have been previously confirmed by correlative investigations of electron microscopy methods and APT that correspond to elemental segregation at dislocations [30,31]. A 1D composition profile that corresponds to a rectangular region of interest (ROI) perpendicular to a representative dislocation, indicated in Fig. 2a (arrow #2), reveals segregation of boron at the dislocation, as shown in Fig. 2d. In addition, molybdenum and carbon are also found to segregate at the same dislocation, as shown in Fig. 2e and 2f, respectively. In some cases, the observed features are found to be unexpectedly interrupted withing the analysed APT volume. It should be noted here that the observed local enrichment is associated with elemental segregation to a dislocation, but not the dislocation

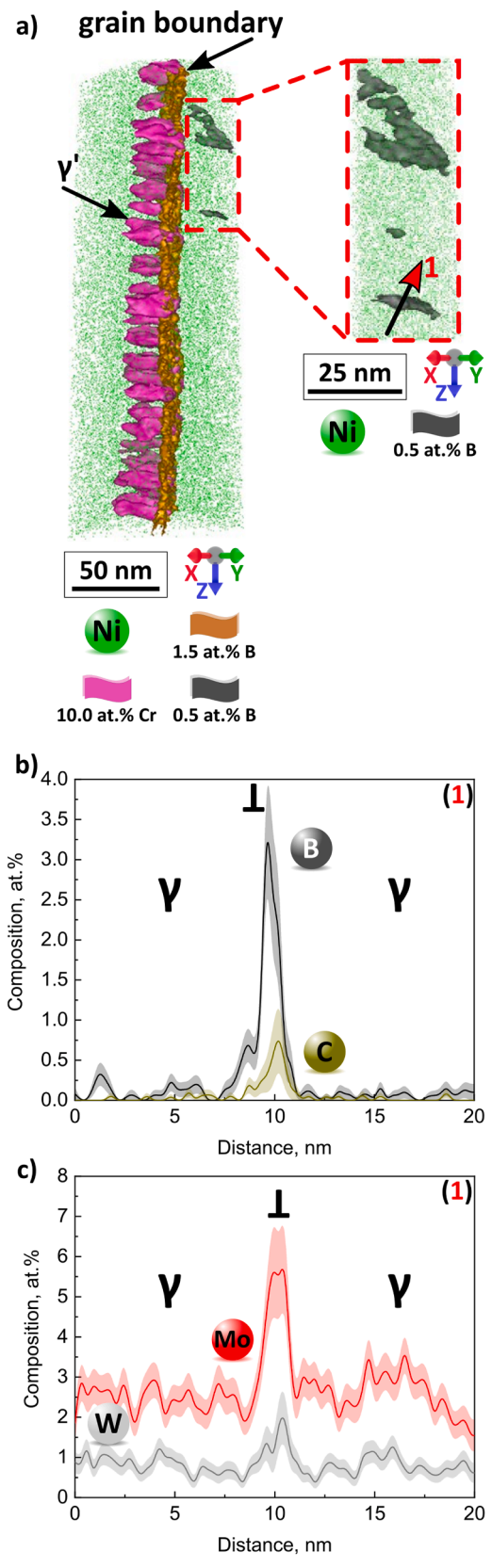

Fig. 4. APT reconstruction from the as-built sample showing dislocations in the vicinity of a grain boundary. b) 1D composition profiles of boron and carbon across the dislocation denoted by arrow #1 in 4a. c) 1D composition profiles of molybdenum and tungsten across the dislocation denoted by arrow #1 in 4a. Error bars are shown as lines filled with colour and correspond to the 2σ counting error.

itself, given the fact that dislocations cannot be directly distinguished by APT. Thus, it is possible to only image the segments of the dislocations which are chemically decorated, as the segregation and diffusion of solutes is perhaps not entirely completed. In particular, the dislocations in the as-built sample have been exposed to elevated temperatures, that allow diffusion of solutes, for relatively short time given the AM processing route. Thus, sufficient time for segregation and diffusion of solutes at dislocations is an important factor to be considered at such phenomena. Also, in the case of the dislocation profile, the rectangular ROI is placed across only within the dislocation as indicated by the isosurface. This allows us to investigate only the atoms segregating at the dislocations. If the width of the ROI is much larger, then it includes a very much higher amount of atoms from the surrounding matrix, and as a consequence the local segregation is averaged out and not observed at first, as it can be seen in Fig. 2c.

Segregation of solutes at dislocations has been previously observed by TEM and APT in superalloys deformed under creep and fatigue at elevated temperatures [32–36], but also after thermomechanical processing [37]. However, in all these cases the observed segregation refers only to dislocations within γ′, but never in the γ matrix. Several hypotheses have been discussed in a recent viewpoint article [19]. amongst them, a scenario can potentially involve the diffusion of solutes out of the dislocations during the slow cooling after for instance creep or fatigue experiments. However, in the case of L-PBF, cooling rates are much higher, thus the segregated solutes at the elevated temperatures can potentially remain trapped after cooling. In the present case, B segregation at dislocations in the as-built condition is thought to result from the interplay between solute partitioning inherited from solidification and dislocation generation upon cooling. Indeed, B is found to partition in the interdendritic region because it is rejected in the residual liquid films during the last stages of solidification. Dislocations are assumed to be created once the solidification is completed, i.e. after “bridging” of the cellular dendrites. The latter idea is supported by our STEM images in Fig. 2a-b where planar dislocations are observed to cross multiple cellular dendrites. Thus, a possible scenario accounting for B segregation at dislocations in the as-built conditions is a solute drag effect. Some solutes would segregate at dislocations resulting in pinning of the dislocations and eventually leading to the stabilization of the dislocation network. This is only a hypothesis and further investigations are required to undoubtedly identify the mechanism accounting for B segregation at dislocations in the as-built microstructure.

Regarding the type of solutes segregating at the dislocation, chromium and cobalt are the most common solutes segregating at dislocations within γ′ precipitates, but this is not the case here. Boron has only been found before to segregate at dislocations in nickel aluminides with a near stoichiometric Ni_3Al composition, but not in the γ matrix [38]. Molybdenum has been found before at dislocations in γ′ [39], which is similar to the dislocations in the γ matrix observed in this study. As the segregation is often related to the minimization of the free energy of the defect within a given phase and based on the fact that now the dislocations are observed in a γ matrix and not within γ′, these can potentially rationalize the different types of solutes segregating at the dislocations. For instance, APT revealed that nickel and cobalt segregate at dislocations within Cr-rich borides after creep, which contradicts the observations made for segregation of solutes at dislocations in γ′ [40].

To unambiguously confirm the segregation of boron at dislocations, further APT investigations were performed. In Fig. 3a, another APT reconstruction is shown, where segregation of boron at dislocations is once again evidenced. This can be seen in the 1D composition profile in Fig. 3b, that corresponds to a cylindrical region perpendicular to the denoted dislocation (arrow #1 in Fig. 3a). In this case, segregation of molybdenum and carbon was not clear. Besides, a 2D contour map of titanium, did not reveal any particular compositional variation over several hundreds of nanometers contrary to Fig. 2a. The relative homogeneity of the spatial distribution of Ti in this region and the average titanium content measured here (Ti ≈ 3.5 at.%) suggests that this

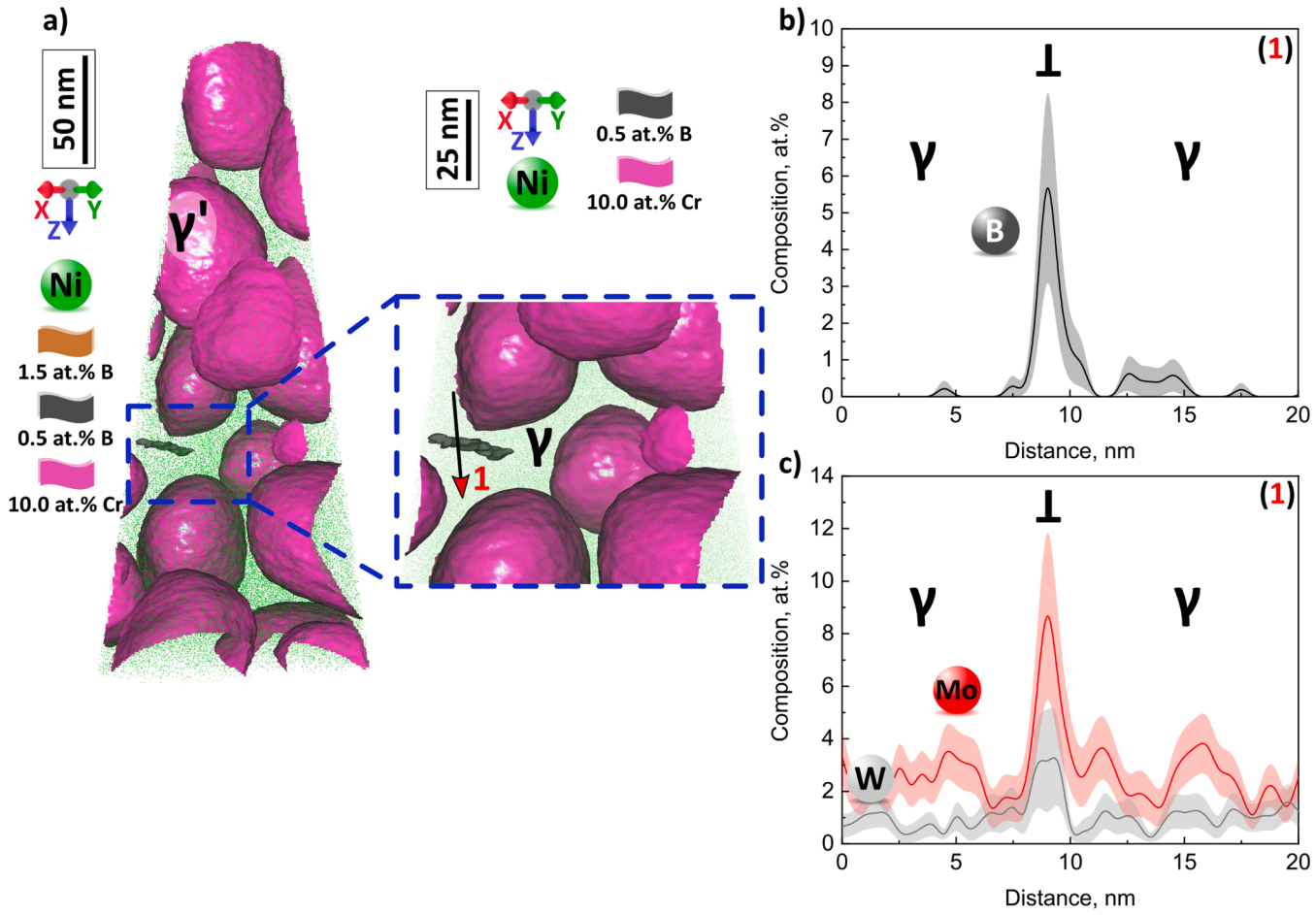

Fig. 5. a) APT reconstruction from the heat-treated sample showing γ′ precipitates and a dislocation in γ matrix. b) 1D composition profile of boron across the dislocation denoted by arrow #1 in 5a. c) 1D composition profile of molybdenum and tungsten across the dislocation denoted by arrow #1 in 5a. Error bars are shown as lines filled with colour and correspond to the 2σ counting error.

analysed volume corresponds to an area from within the dendrite core. The observation of dislocations in the dendrite core decorated by boron, can further support the scenario that solute drag effects occur as dislocations cross multiple cellular dendrites.

Dislocations were also found in the vicinity of grain boundaries. An APT reconstruction from the as-built sample containing a grain boundary and dislocations is shown in Fig. 4. In this case, a 1D composition profile denoted as #1 in Fig. 4a, shows a clear segregation of boron, molybdenum and carbon at a dislocation, as shown previously. Besides, a segregation of tungsten is also observed in this case. Segregation of tungsten at dislocations has been previously assumed for a superalloy, but not proven, as a result of the precipitation of tungsten rich M_6C carbides in high dislocation density regions after very high cycle fatigue deformation [35]. Note that here, γ′ precipitates are only present at the grain boundaries, which have been investigated and confirmed by TEM in a different study [41].

After heat treatment, TEM investigations revealed that dislocations are not completely removed from the microstructure, given that a subsolvus solution treatment was applied. Thus, we aimed to investigate potential segregation of solutes at dislocations after the heat treatment and examine whether there is a change in the segregation character. Fig. 5a shows an APT reconstruction that contains γ′ precipitates formed after the full heat treatment. In the γ matrix, a tubular feature, similar to what has been observed in the as-built sample, can be observed. A 1D composition profile across the dislocation, shows a clear segregation of boron, molybdenum and tungsten, Fig. 5b and 5c. The segregation character is the same in terms of what solutes segregate at the dislocations. However, there is a slight difference in their amounts. For instance, in the as-built sample, the maximum amount of boron at the dislocation was up to 2.5 at.%, while in the heat treated sample raises up to 5.5 at.%. Similarly, the maximum observed amount of molybdenum increases from 5.5 at.% in the as-built sample to up to 9.0 at.% in the heat treated sample. A significant increase is not measured in the case of tungsten, while carbon was not found at the dislocation in the heat-treated sample.

In this study the focus is not placed on the amount of solute segregation at dislocations, but on what solutes partition at dislocation. However, this difference in the amount of solutes at dislocations observed in the as-built and heat-treated alloy could be related to various phenomena. For instance, the observed segregation could be correlated to different types of dislocations, i.e. screw or edge, thus resulting to different amount of solutes [19]. To gain such information, a correlative TEM/APT study is required. In this case, at the same specimen, TEM would provide information regarding the type of dislocation and subsequently compositional information would be collected by APT. However, given the geometry of the APT samples, which restricts analyses on the type of dislocations, a sample preparation protocol that exploits the strengths of both these characterization methods in the case of dislocations has not been developed. Such protocols, however, have been developed for other types of crystal defects [31]. In addition, another factor that should be considered is that dislocations are not necessarily generated at the same time. This leads to shorter or longer times for the solutes to segregate at dislocations and result in the observed differences. Besides, after heat treatment the annealing of

some dislocations led to a reduced available number of sites where trapping of these solutes can occur, thus the segregating solutes can be concentrated in the fewer dislocations.

Segregation and trapping of boron at dislocations during L-PBF processes can have implications on their microstructural evolution but also on their design and processing. For instance, segregation of boron and molybdenum can potentially contribute to stabilizing the network of dislocations, especially in the as-built microstructure and lead to the formation of borides during heat treatment. It is well known that boron combines with molybdenum to form borides in superalloys [42,43]. In this alloy such Mo-rich borides have been observed after heat treatment in a different study [41]. The borides were almost exclusively observed at the grain boundaries, while the STEM observations in the heat-treated microstructure did not reveal any formation of borides at the remaining dislocations (Fig. 1). Intergranular borides are often desirable due to their beneficial effect on high temperature deformation [3,40,44], however there are some cases at which borides act as dislocation sources that can have a detrimental effect to the mechanical properties [45,46].

Recently, direct ageing has been considered for L-PBF alloys, where a solution treatment step is not required as it is assumed that there is a supersaturated matrix [47,48]. In such scenario, a significant proportion of dislocations will not be removed, and some boron may remain trapped at dislocations, possibly leading to low amounts of boron available to finally segregate at grain boundaries and strengthen them. But, by reducing the dislocation density through a full heat treatment process, a higher amount of boron will diffuse towards the grain boundaries, which was shown in a previous study [49]. In particular, APT have shown that the amount of boron was up to 2.0 at.% in a high angle grain boundary in the as-built condition, while increased up to 6.0 at.% after heat treatment. The creep performance at 650 °C of the AM produced alloy was compared to that manufactured by cast and wrought processes (Fig. 1 in [41]). Although the creep performance of the AM alloy was deteriorated, this was attributed to the presence of cracks in the initial microstructure and not to lower amounts of boron at grain boundaries.

A careful design and understanding of boron trapping at dislocations could be used potentially as a mechanism to mitigate hot cracking during L-PBF processing, by reducing the available amount of boron segregating at grain boundaries, thus hindering hot cracking. However, this hypothesis must be questioned since it is not clear at what stage the dislocations are generated. As most likely dislocations are generated once the solidification is completed, this hypothesis would require further development and investigations, for instance by exploring the effect of solution treatment temperature on the dislocation density and boron segregation at grain boundaries.

4. Summary and conclusions

In summary, our results demonstrate that boron, amongst other solutes, can be trapped at dislocations during the L-PBF processing of the AD730® superalloy. APT revealed segregation of boron, molybdenum and in some instance carbon at dislocations in the γ matrix of the as-built condition. This observation was made for dislocations located both in the interdendritic regions and dendrite cores. After a sub-solvus heat treatment, the dislocation density has been reduced but not completely removed as shown by TEM. The remaining dislocations were also found decorated with boron and molybdenum and to relatively higher amounts compared to those in the as-built condition. The observed boron trapping can potentially influence not only the additive manufacturing processes of nickel-based superalloys but also their alloy design guidelines.

Declaration of Competing Interests

The authors declare that they have no known competing financial interests or personal relationships that could have appeared to influence the work reported in this paper.

Acknowledgements

This work was financially supported by Aubert & Duval as part of the SOFIA project (BPI France) and has benefited from the equipment of the Grenoble INP - CMTC platform supported by the Centre of Excellence of Multifunctional Architectured Materials “CEMAM” n°ANR-10-LABX-44–01. S.A. would like to acknowledge financial support from the Alexander Humbolt foundation. Uwe Tezins and Andreas Sturm are acknowledged for their support to the FIB & APT facilities at MPIE.

References

[1] F. Theska, R. Buerstmayr, H. Liu, M. Lison-Pick, S.R. Street, S. Primig, Influence of grain boundary precipitation and segregation on cracking of cast and wrought superalloys containing B and Zr, Mater. Charact. 187 (2022), 111881.
[2] D. Tytko, P.-P. Choi, J. Klöwer, A. Kostka, G. Inden, D. Raabe, Microstructural evolution of a Ni-based superalloy (617B) at 700°C studied by electron microscopy and atom probe tomography, Acta Mater 60 (2012) 1731–1740.
[3] P. Kontis, H.A.M. Yusof, S. Pedrazzini, M. Danaie, K.L. Moore, P.A.J. Bagot, M. P. Moody, C.R.M. Grovenor, R.C. Reed, On the effect of boron on grain boundary character in a new polycrystalline superalloy, Acta Mater 103 (2016) 688–699.
[4] Q. Wang, Y. Wu, J. Chen, J. Song, C. Xiao, X. Hui, Enhancement of high temperature low cycle fatigue lifetime of PWA1484 superalloy artificial bicrystals via boron-induced grain boundary strengthening, Int. J. Fatigue. 165 (2022), 107223.
[5] F. Theska, W.F. Tse, B. Schulz, R. Buerstmayr, S.R. Street, M. Lison-Pick, S. Primig, Review of microstructure–mechanical property relationships in cast and wrought ni-based superalloys with boron, carbon, and zirconium Microalloying additions, Adv. Eng. Mater. (2022), 2201514.
[6] T. Alam, P.J. Felfer, M. Chaturvedi, L.T. Stephenson, M.R. Kilburn, J.M. Cairney, Segregation of B, P, and C in the Ni-based superalloy, inconel 718, Metall. Mater. Trans. A. 43 (2012) 2183–2191.
[7] X.B. Hu, Y.L. Zhu, X.L. Ma, Crystallographic account of nano-scaled intergrowth of M 2 B-type borides in nickel-based superalloys, Acta Mater 68 (2014) 70–81.
[8] H.R. Zhang, O.A. Ojo, M.C. Chaturvedi, Nanosize boride particles in heat-treated nickel base superalloys, Scr. Mater. 58 (2008) 167–170.
[9] H.-R. Zhang, O.A. Ojo, Cr-rich nanosize precipitates in a standard heat-treated Inconel 738 superalloy, Philos. Mag. 90 (2010) 765–782.
[10] D. Blavette, P. Duval, L. Letellier, M. Guttmann, Atomic-scale APFIM and TEM investigation of grain boundary microchemistry in astroloy nickel base superalloys, Acta Mater 44 (1996) 4995–5005.
[11] R. Gupta, K.C.H. Kumar, M.J.N.V. Prasad, P. Pant, Compositionally graded nano-sized borides in a directionally solidified nickel-base superalloy, Scr. Mater. 201 (2021), 113981.
[12] J. Grodzki, N. Hartmann, R. Rettig, E. Affeldt, R.F. Singer, Effect of B, Zr, and C on hot tearing of a directionally solidified nickel-based superalloy, Metall. Mater. Trans. A. 47 (2016) 2914–2926.
[13] H. Gruber, E. Hryha, K. Lindgren, Y. Cao, M. Rashidi, L. Nyborg, The effect of boron and zirconium on the microcracking susceptibility of IN-738LC derivatives in laser powder bed fusion, Appl. Surf. Sci. 573 (2022), 151541.
[14] K. Lindgren, F. Schulz, H. Gruber, A. Markström, E. Hryha, On the role of Zr and B addition on solidification cracking of IN738LC produced by laser powder bed fusion, Materialia 26 (2022), 101609.
[15] Y. Zhao, Z. Ma, L. Yu, Y. Liu, New alloy design approach to inhibiting hot cracking in laser additive manufactured nickel-based superalloys, Acta Mater 247 (2023), 118736.
[16] E.B. Raeker, K.M. Pusch, S.A.J. Forsik, N. Zhou, A.D. Dicus, Q.Q. Ren, J. D. Poplawsky, M.M. Kirka, T.M. Pollock, Minor elements and solidification cracking during laser powder-bed fusion of a high γ′ CoNi-Base superalloy, Metall. Mater. Trans. A Phys. Metall. Mater. Sci. 54 (2023) 1744–1757.
[17] A. Hariharan, L. Lu, J. Risse, A. Kostka, B. Gault, E.A. Jägle, D. Raabe, Misorientation-dependent solute enrichment at interfaces and its contribution to defect formation mechanisms during laser additive manufacturing of superalloys, Phys. Rev. Mater. 3 (2019), 123602.
[18] F. Deirmina, S. Koenig, M. Hasselqvist, E. Oscarsson, O. Adegoke, N.H. Pettersson, M. Pellizzari, Influence of boron on the stress-rupture behavior of an additively manufactured Hastelloy X, Mater. Sci. Eng. A. 863 (2023), 144483.
[19] P. Kontis, Interactions of solutes with crystal defects: a new dynamic design parameter for advanced alloys, Scr. Mater. 194 (2020), 113626.
[20] T.G. Gallmeyer, S. Moorthy, B.B. Kappes, M.J. Mills, B. Amin-Ahmadi, A. P. Stebner, Knowledge of process-structure-property relationships to engineer better heat treatments for laser powder bed fusion additive manufactured Inconel 718, Addit. Manuf. 31 (2020), 100977.
[21] T. Vilaro, C. Colin, J.D. Bartout, L. Nazé, M. Sennour, Microstructural and mechanical approaches of the selective laser melting process applied to a nickel-base superalloy, Mater. Sci. Eng. A. 534 (2012) 446–451.
[22] X. Wang, L.N. Carter, B. Pang, M.M. Attallah, M.H. Loretto, Microstructure and yield strength of SLM-fabricated CM247LC Ni-Superalloy, Acta Mater 128 (2017) 87–95.
[23] K. Thompson, D. Lawrence, D.J. Larson, J.D. Olson, T.F. Kelly, B. Gorman, In situ site-specific specimen preparation for atom probe tomography, Ultramicroscopy 107 (2007) 131–139.

[24] J. Xu, P. Kontis, R.L. Peng, J. Moverare, Modelling of additive manufacturability of nickel-based superalloys for laser powder bed fusion, Acta Mater 240 (2022), 118307.
[25] A. De Luca, C. Kenel, S. Griffiths, S.S. Joglekar, C. Leinenbach, D.C. Dunand, Microstructure and defects in a Ni-Cr-Al-Ti γ/γ' model superalloy processed by laser powder bed fusion, Mater. Des. 201 (2021), 109531.
[26] Z. Sun, Y. Ma, D. Ponge, S. Zaefferer, E.A. Jägle, B. Gault, A.D. Rollett, D. Raabe, Thermodynamics-guided alloy and process design for additive manufacturing, Nat. Commun. 13 (2022) 1–12, 2022 131.
[27] H.T. Pang, H.J. Stone, C.M.F. Rae, L. Zhang, R.A. Hobbs, Solution heat treatment optimization of fourth-generation single-crystal nickel-base superalloys, Metall. Mater. Trans. A Phys. Metall. Mater. Sci. 43 (2012) 3264–3282.
[28] V.C.I. Strutt, B.M. Jenkins, J.M. Woolrich, M. Appleton, M.P. Moody, P.A.J. Bagot, Effect of microsegregation and heat treatment on localised γ and γ' compositions in single crystal Ni-based superalloys, J. Alloys Compd. 949 (2023), 169861.
[29] A. Després, C. Mayer, M. Veron, E.F. Rauch, M. Bugnet, J.J. Blandin, G. Renou, C. Tassin, P. Donnadieu, G. Martin, On the variety and formation sequence of second-phase particles in nickel-based superalloys fabricated by laser powder bed fusion, Materialia 15 (2021), 101037.
[30] M. Kuzmina, M. Herbig, D. Ponge, S. Sandlobes, D. Raabe, Linear complexions: confined chemical and structural states at dislocations, Science 349 (2015) 1080–1083.
[31] S.K. Makineni, M. Lenz, P. Kontis, Z. Li, A. Kumar, P.J. Felfer, S. Neumeier, M. Herbig, E. Spiecker, D. Raabe, B. Gault, Correlative microscopy—novel methods and their applications to explore 3D chemistry and structure of nanoscale lattice defects: a case study in Superalloys, JOM 70 (2018) 1736–1743.
[32] T.M. Smith, B.D. Esser, N. Antolin, A. Carlsson, R.E.A. Williams, A. Wessman, T. Hanlon, H.L. Fraser, W. Windl, D.W. McComb, M.J. Mills, Phase transformation strengthening of high temperature superalloys, Nat. Commun. 7 (2016) 1–7.
[33] S. Antonov, Y. Zheng, J.M. Sosa, H.L. Fraser, J. Cormier, P. Kontis, B. Gault, Plasticity assisted redistribution of solutes leading to topological inversion during creep of superalloys, Scr. Mater. 186 (2020) 287–292.
[34] L. Lilensten, S. Antonov, B. Gault, S. Tin, P. Kontis, Enhanced creep performance in a polycrystalline superalloy driven by atomic-scale phase transformation along planar faults, Acta Mater 202 (2021) 232–242.
[35] A. Cervellon, S. Hémery, P. Kürnsteiner, B. Gault, P. Kontis, J. Cormier, Crack initiation mechanisms during very high cycle fatigue of Ni-based single crystal superalloys at high temperature, Acta Mater 188 (2020) 131–144.
[36] T.M. Smith, B.S. Good, T.P. Gabb, B.D. Esser, A.J. Egan, L.J. Evans, D.W. McComb, M.J. Mills, Effect of stacking fault segregation and local phase transformations on creep strength in Ni-base superalloys, Acta Mater 172 (2019) 55–65.
[37] S. Katnagallu, S. Vernier, M.-A. Charpagne, B. Gault, N. Bozzolo, P. Kontis, Nucleation mechanism of hetero-epitaxial recrystallization in wrought nickel-based superalloys, Scr. Mater. 191 (2021) 7–11.
[38] M.K. Miller, J.A. Horton, Direct observation of boron segregation to line and planar defects in Ni3Al, J. Phys. Colloq. 48 (1987). C6-379-C6-384.
[39] X. Wu, S.K. Makineni, P. Kontis, G. Dehm, D. Raabe, B. Gault, G. Eggeler, On the segregation of *Re* at dislocations in the γ' phase of Ni-based single crystal superalloys, Materialia 4 (2018) 109–114.
[40] L. Lilensten, A. Kostka, S. Lartigue-Korinek, B. Gault, S. Tin, S. Antonov, P. Kontis, Partitioning of solutes at crystal defects in borides after creep and annealing in a polycrystalline superalloy, JOM 73 (2021) 2293–2302.
[41] A. Després, S. Antonov, C. Mayer, C. Tassin, M. Veron, J.J. Blandin, P. Kontis, G. Martin, On the role of boron, carbon and zirconium on hot cracking and creep resistance of an additively manufactured polycrystalline superalloy, Materialia 19 (2021), 101193.
[42] P.A.J. Bagot, O.B.W. Silk, J.O. Douglas, S. Pedrazzini, D.J. Crudden, T.L. Martin, M. C. Hardy, M.P. Moody, R.C. Reed, An atom probe tomography study of site preference and partitioning in a nickel-based superalloy, Acta Mater 125 (2017) 156–165.
[43] P. Kontis, A. Kostka, D. Raabe, B. Gault, Influence of composition and precipitation evolution on damage at grain boundaries in a crept polycrystalline Ni-based superalloy, Acta Mater 166 (2019) 158–167.
[44] B.C. Yan, J. Zhang, L.H. Lou, Effect of boron additions on the microstructure and transverse properties of a directionally solidified superalloy, Mater. Sci. Eng. A. 474 (2008) 39–47.
[45] R.R. Unocic, N. Zhou, L. Kovarik, C. Shen, Y. Wang, M.J. Mills, Dislocation decorrelation and relationship to deformation microtwins during creep of a γ′ precipitate strengthened Ni-based superalloy, Acta Mater 59 (2011) 7325–7339.
[46] H.L. Ge, J.D. Liu, S.J. Zheng, Y.T. Zhou, Q.Q. Jin, X.H. Shao, B. Zhang, Y.Z. Zhou, X.L. Ma, Boride-induced dislocation channeling in a single crystal Ni-based superalloy, Mater. Lett. 235 (2019) 232–235.
[47] M. Pröbstle, S. Neumeier, J. Hopfenmüller, L.P. Freund, T. Niendorf, D. Schwarze, M. Göken, Superior creep strength of a nickel-based superalloy produced by selective laser melting, Mater. Sci. Eng. A. 674 (2016) 299–307.
[48] Y.T. Tang, J.N. Ghoussoub, C. Panwisawas, D.M. Collins, S. Amirkhanlou, J.W. G. Clark, A.A.N. Németh, D.Graham McCartney, R.C. Reed, The effect of heat treatment on tensile yielding response of the new superalloy ABD-900AM for additive manufacturing, Miner. Met. Mater. Ser. (2020) 1055–1065.
[49] A. Després, S. Antonov, C. Mayer, M. Veron, E.F. Rauch, C. Tassin, J.-J. Blandin, P. Kontis, G. Martin, Revealing the true partitioning character of zirconium in additively manufactured polycrystalline superalloys, Addit. Manuf. Lett. 1 (2021), 100011.